Real-time analysis of the role of Ca^{2+} in flagellar movement and motility in single sea urchin sperm

Christopher D. Wood,[1] Takuya Nishigaki, [1] Toshiaki Furuta,[2] Shoji A. Baba,[3] and Alberto Darszon[1]

[1]Department of Developmental Genetics and Molecular Physiology, Institute of Biotechnology, National Autonomous University of Mexico (UNAM), Cuernavaca, Morelos 62210, Mexico
[2]PRESTO, JST and Department of Biomolecular Science, Toho University, Funabashi 274-8510, Japan
[3]Department of Biology, Ochanomizu University, Tokyo 112-8610, Japan

Eggs of many marine and mammalian species attract sperm by releasing chemoattractants that modify the bending properties of flagella to redirect sperm paths toward the egg. This process, called chemotaxis, is dependent on extracellular Ca^{2+}. We used stroboscopic fluorescence imaging to measure intracellular Ca^{2+} concentration ($[Ca^{2+}]i$) in the flagella of swimming sea urchin sperm. Uncaging of cyclic GMP induced Ca^{2+} entry via at least two distinct pathways, and we identified a nimodipine-sensitive pathway, compartmentalized in the flagella, as a key regulator of flagellar bending and directed motility changes. We found that, contrary to current models, the degree of flagellar bending does not vary in proportion to the overall $[Ca^{2+}]i$. Instead we propose a new model whereby flagella bending is increased by Ca^{2+} flux through the nimodipine-sensitive pathway, and is unaffected by $[Ca^{2+}]i$ increases through alternative pathways.

Introduction

The likelihood of sperm–egg encounter is enhanced in many marine and mammalian species by secretion of chemoattractant molecules by the egg or its associated structures (Eisenbach, 1999). Sea urchin sperm are a useful model for studying chemotaxis, and flagellar-driven motility in general, as the sperm swim with a plane circular trajectory of ~50-μm diameter for extended periods. This is due to their flagella beating in near-planar waves that are displaced to one side in relation to the long axis of the head (Cosson et al., 2003). In the presence of a concentration gradient of chemoattractant, sperm from the sea urchin *Arbacia punctulata* undergo a series of brief turns interspersed by periods of straighter swimming that direct them toward the source of the stimulus (Miller, 1985; Ward et al., 1985; Kaupp et al., 2003). The turns are generated by brief increases in flagellar asymmetry that elevate the acute angle between the long axes of the head and of the flagellum (Miller and Brokaw, 1970).

External Ca^{2+} is an essential requirement for chemotaxis (Brokaw, 1974; Cosson et al., 1984; Ward et al., 1985; Spehr et al., 2003). Most models propose that chemoattractants regulate flagellar asymmetry by stimulating the entry of external Ca^{2+} (Cook et al., 1994; Kaupp et al., 2003; Ishikawa et al., 2004), and chemoattractants have been shown to increase intracellular calcium concentration ($[Ca^{2+}]i$) in cell populations (Cook et al., 1994; Kaupp et al., 2003) and immobilized single sperm (Spehr et al., 2003). It is also known that the Ca^{2+} concentration is proportionately related to the degree of flagellar asymmetry in demembranated sea urchin sperm flagella (Brokaw, 1979). Whether this is true for intact flagella is unknown, and dynamic agonist-stimulated Ca^{2+} changes in the beating flagella of individual motile sperm have not been measured directly.

Resact, a 14-aa sperm-activating peptide (SAP) isolated from the egg outer investments of *A. punctulata*, is the only sea urchin chemoattractant that has been definitively identified to date (Ward et al., 1985; Kaupp et al., 2003). The initial resact-stimulated signaling event is a transient increase in cyclic guanosine monophosphate (cGMP) (Suzuki and Garbers, 1984; Shimomura and Garbers, 1986; Kaupp et al., 2003). Uncaging of cGMP has been reported to induce chemotaxis-like motility changes in *A. punctulata* sperm (Kaupp et al., 2003). We decided to investigate whether the same cGMP-stimulated changes in motility occur in *Strongylocentrotus purpuratus* sperm, while simultaneously measuring $[Ca^{2+}]i$ changes in the flagella.

Results and discussion

S. purpuratus sperm were loaded with caged cGMP and the Ca^{2+} indicator dye fluo-4. Fluorescence microscopy was used

Correspondence to Christopher D. Wood: chris@ibt.unam.mx

Abbreviations used in this paper: ASW, artificial sea water; $[Ca^{2+}]i$, intracellular calcium concentration; Ca_v, voltage-gated Ca^{2+}; cGMP, cyclic guanosine monophosphate; DHP, dihydropyridine; SAP, sperm-activating peptide.

The online version of this article includes supplemental material.

The Journal of Cell Biology, Vol. 169, No. 5, June 6, 2005 725–731
http://www.jcb.org/cgi/doi/10.1083/jcb.200411001

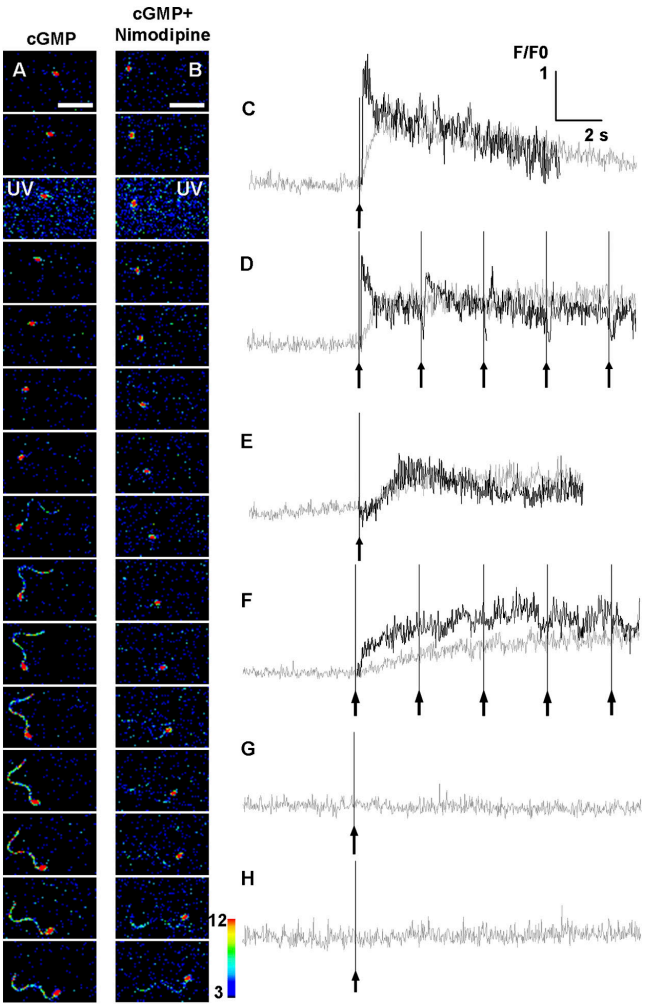

Figure 1. **Uncaging cGMP increases Ca^{2+} in swimming sperm.** (A and B) Fluorescence images of caged cGMP- and fluo-4–loaded sperm before and after UV flash in (A) ASW and (B) ASW containing 30 μM nimodipine. Interval between images = 23 ms. Bars, 20 μm. Color bar shows fluorescence intensity after background subtraction. (C–H) Normalized increases in fluo-4 fluorescence (F/F_0) in flagellum (black) and head (gray) of individual swimming sperm after uncaging of cGMP. Arrow with line denotes UV flash. (C and D) ASW, (E and F) ASW with 30 μM nimodipine, (G) ASW with 50 mM K^+, (H) zero Ca^{2+} ASW. Video 1 shows animated sequence of images in A and B (Video 1 available at http://www.jcb.org/cgi/content/full/jcb.200411001/DC1).

to monitor sperm swimming in circles in artificial sea water (ASW) at the water–coverslip boundary within the microscope field for up to 20 s. At resting $[Ca^{2+}]i$ only the fluorescence signal from the head could normally be detected (Fig. 1 A, topmost panels). Upon uncaging of cGMP by a single UV flash and after a brief delay (125 ± 5 ms, $n = 52$; Table I), a rapid and sustained increase in $[Ca^{2+}]i$ was observed in the flagella and head (Fig. 1 A; Video 1, available at http://www.jcb.org/cgi/content/full/jcb.200411001/DC1). In the flagella, $[Ca^{2+}]i$ increases were biphasic in nature, with a fast initial component ($t_{1/2}$ increase = 48 ± 7 ms, $n = 23$; Table I) that was followed by a slowly declining plateau phase (Fig. 1 C). In the head, $[Ca^{2+}]i$ increases lacked the fast component, rising more slowly to the plateau phase ($t_{1/2}$ = 644 ± 65 ms, $n = 52$; Table I). Repetitive application of UV flashes induced successive transient increases in $[Ca^{2+}]i$ in the flagella (Fig. 1 D). These were superimposed onto the high plateau of Ca^{2+}, and showed successively diminishing amplitudes. Under the same conditions, the plateau levels of $[Ca^{2+}]i$ in the head were more sustained (Fig. 1 D). All phases of the $[Ca^{2+}]i$ increases were abolished in cells swimming in either high K^+ ASW (Fig. 1 G), in which all signaling events downstream of cGMP are inhibited (Harumi et al., 1992), or in zero Ca^{2+} ASW (Fig. 1 H). Interestingly, brief decreases in the flagellar $[Ca^{2+}]i$ that immediately follow secondary UV flashes were recorded in 13 of 23 flagella (Fig. 1 D). This agrees with a recent report detailing these decreases in $[Ca^{2+}]i$ in populations of *S. purpuratus* sperm, and immobilized single sperm, that are generated by a hyperpolarization-stimulated activation of a Na^+/Ca^{2+} exchanger pathway (Nishigaki et al., 2004). Due to the relative infrequency of these decreases in $[Ca^{2+}]i$, their influence (if any) on sperm motility could not be assessed.

Occasionally (4 of 114 sperm) the fluorescence signal from flagella was just barely detectable before the UV flash (unpublished data). In these cells it was confirmed that the flagellar $[Ca^{2+}]i$ was stable and unchanging before stimulation. We also occasionally observed spontaneous $[Ca^{2+}]i$ increases occurring simultaneously in head and flagellar compartments (unpublished data), as has been previously reported to occur in single immobilized sperm (Wood et al., 2003). Such sperm were omitted from the analyses presented here. The average diameter of the circular swimming trajectory in the absence (41 ± 6 μm, $n = 30$) or presence (42 ± 7 μm, $n = 38$) of Pluronic F127 in the dye-loading medium was not significantly different (unpaired *t* test), and sperm incubated with fluo-4 alone did not increase their $[Ca^{2+}]i$, nor alter their trajectories, upon exposure to UV (unpublished data).

We next tried to identify which Ca^{2+} entry pathways were activated by release of cGMP. Addition of 30 μM nimodipine, a dihydropyridine (DHP) frequently used as an inhibitor of voltage-gated Ca^{2+} (Ca_v) channels (for review see Doering and Zamponi, 2003; Yunker, 2003), significantly increased the delay to the $[Ca^{2+}]i$ increase from 125 ± 5 ms (in untreated cells) to 210 ± 12 ms ($n = 22$, $P < 0.05$, Table I; Fig. 1 B; Video 1). In the head, the kinetics of the Ca^{2+} increase were significantly slowed, with the $t_{1/2}$ increasing from 644 ± 65 ms to 1375 ± 150 ms ($n = 29$, $P < 0.05$; Table I). However, the basal $[Ca^{2+}]i$ and the overall relative peak increase in $[Ca^{2+}]i$ were unaffected (Table I). In the flagella the kinetics of the $[Ca^{2+}]i$ increase were significantly slowed, with the $t_{1/2}$ increasing from 48 ± 7 ms to 390 ± 80 ms in nimodipine-treated sperm ($n = 22$, $P < 0.05$; Table I). Nimodipine inhibited the "fast" component of the cGMP-stimulated $[Ca^{2+}]i$ increase in flagella at both initial and successive UV flashes (Fig. 1 F), whereas the sustained phase of the $[Ca^{2+}]i$ was less dramatically affected. This suggests that there are at least two Ca^{2+} entry pathways in sea urchin sperm, and that a nimodipine-sensitive pathway mediates the fast component. The compartmentalization of the fast component of the $[Ca^{2+}]i$ increase to flagella suggests either preferential localization or activation of this pathway at this site. The components of the

Table I. **Effect of various treatments on the increase in [Ca^{2+}]i and motility changes produced by uncaging of cGMP in single sperm**

	Ca^{2+} parameters					Motility parameters			
	Head			Flagella					
	Basal Ca^{2+} (F)	Peak increase in Ca^{2+} ($\Delta F/F_0$)	$t_{1/2}$ increase	Delay to Ca^{2+} increase	$t_{1/2}$ increase	Basal velocity	% change in velocity	Basal curvature $\times 10^{-3}$	% average change in curvature
		%	*ms*	*ms*	*ms*	*μm/s*		*(rad/μm)*	
Untreated (52)	18 ± 1.3	124 ± 8	644 ± 65	125 ± 5	48 ± 7[c]	165 ± 4	6.7 ± 1.0	54 ± 1	34.7 ± 3.2
Nimodipine (29)	23 ± 2.1	104 ± 7	1375 ± 150[a]	210 ± 12[a]	390 ± 80[a,d]	128 ± 3[a,b]	11.1 ± 1.5[b]	47 ± 2[a,b]	−1.1 ± 0.9[a]
Zero Ca^{2+} (23)	-	-	-	-	-	180 ± 5	13.2 ± 2.5[a,b]	46 ± 2[a,b]	−6.5 ± 2.1[a]
High K^+ (12)	17 ± 4.3	-	-	-	-	180 ± 6	−1.2 ± 0.5[a]	60 ± 2	3.6 ± 1.7[a]
Ni^{2+} (12)	12 ± 1	57 ± 12[a]	1960 ± 420[a]	345 ± 30[a]	160 ± 30[e]	205 ± 5[a]	9.3 ± 2.1[b]	50 ± 1	−0.6 ± 3.7[a]

All sperm were loaded with equal concentrations of fluo-4-AM and Bhc-cGMP/Ac. Untreated, sperm in ASW; Nimodipine, ASW containing 30 μM nimodipine; Zero Ca^{2+}, zero Ca^{2+} ASW; High K^+, ASW containing 50 mM K^+; Ni^{2+}, ASW containing 100–200 μM Ni^{2+}. Number in parentheses = number of cells analyzed. Category titles and symbols used: Basal Ca^{2+} is the average-per-pixel raw fluorescence intensity value from the head over 5 s before UV flash; ΔF is the amplitude of increase in fluorescence intensity between basal and peak values, F_0 is the basal average fluorescence intensity value; $t_{1/2}$ is the time taken to reach half the peak fluorescence, measured from the first appearance of the flagellum in the digital image series; Delay to Ca^{2+} increase measured from the time of UV flash until the first appearance of the flagellum in the digital image series; Basal velocity is the average velocity over 5 s before UV flash; Change in velocity measured from an average velocity over 100 frames (2.3 s) after UV flash, and the basal velocity; Basal curvature is the average curvature over 5 s before UV flash; Change in curvature measured from an average curvature in 10 frames (230 ms) after UV flash, and the basal curvature.
[a]Significantly different from untreated cells (see Materials and methods).
[b]Significantly different from 50 mM K^+ treated cells (see Materials and methods).
[c]Number of flagella analyzed = 23.
[d]Number of flagella analyzed = 22.
[e]Number of flagella analyzed = 12. All other values not significantly different within respective category. Values stated as ± SEM.

Ca^{2+} entry pathway involved in the sustained phase appear more widely distributed. This latter pathway might be an as-yet poorly characterized SAP-stimulated, cAMP-mediated Ca^{2+} entry mechanism(s) (Cook and Babcock, 1993; Kaupp et al., 2003; Wood et al., 2003; Nishigaki et al., 2004). Treatment of sperm with 100–200 μM Ni^{2+}, previously used to inhibit Ca^{2+} entry during the acrosome reaction in sea urchin sperm (Gonzalez-Martinez et al., 2001), also slowed the kinetics of the [Ca^{2+}]i increase in both flagella and head (Table I).

We then examined the consequences of manipulating the Ca^{2+} entry pathways on motility. Uncaging of cGMP induced sperm to undergo a transient fast turn (average % increase in curvature = 34.7 ± 3.2%, n = 52; Table I), followed by a return to a circular path of increased diameter (in comparison to the pre-flash trajectory; Fig. 2 a; Video 2, available at http://www.jcb.org/cgi/content/full/jcb.200411001/DC1). This was accompanied by a 6.7 ± 1% average increase in velocity (n = 52, Table I; Fig. S1, available at http://www.jcb.org/cgi/content/full/jcb.200411001/DC1). The turning events are created by transient (40–80 ms) increases in the asymmetry of the flagella that increase the acute angle between the long axes of the head and flagellum (Fig. 3 a). Successive UV flashes produced a corresponding series of diminishing turns (Fig. 2 b), each of which was also the product of transient increases in flagellar asymmetry (Fig. 3 b). The characteristics of these transient changes in flagellar asymmetry were not altered by any potential fluo-4–dependent buffering artifacts (Fig. S2). The combination of a turn followed by a period of straighter swimming resulted in a directed relocation of the sperm path along a "flash axis" (see Fig. 4 a and its legend for definition). This directed relocation was greater at the first UV flash than at subsequent, secondary UV flashes (Fig. 4 b). In high K^+ ASW, all components of the cGMP-stimulated motility changes (i.e., the turning events, the straighter trajectories, the increase in velocity, and the directed relocation) are inhibited (Fig. 2 d, Fig. 4 d; Table I; Fig. S1). In zero Ca^{2+} ASW, uncaging cGMP increased both the velocity of the sperm and the diameter of the sperm trajectory, while the turning events and directed relocation along the flash axis were absent (Fig. 2 e, Fig. 4 e; Table I; Fig. S1). In contrast to sperm in ASW, after the first UV flash there was a tendency for sperm in zero Ca^{2+} ASW to relocate perpendicularly to the flash axis. This was due to the consistent delay between cGMP release and the increase in diameter of the sperm trajectory. As external Ca^{2+} is a known requirement for chemotaxis, and this increase in diameter is triggered only at the first UV flash, and not at subsequent UV flashes, we consider it unlikely that the switch to a trajectory of increased diameter alone could be a potential chemotactic mechanism.

Thereafter we studied the effect of nimodipine on the motility of cGMP-stimulated sperm. Uncaging cGMP in nimodipine-treated sperm increased their average velocity (11.1 ± 1.5%, n = 29, Table I; Fig. S1), and they swam in circles of greater diameter (Fig. 2 c). However, the turning events were absent, both at the first UV flash (average % change in curvature = −1.1 ± 0.9%, n = 29; Table I) and upon the application of secondary flashes (Fig. 2 c; Video 3, available at http://www.jcb.org/cgi/content/full/jcb.200411001/DC1). This was due to the absence of the brief increases in flagellar asymmetry seen in untreated sperm (Fig. 3 c). Nimodipine treatment also abolished the directed relocation of the swimming paths along the flash axis observed in untreated sperm (Fig. 4 c). As with sperm swimming in zero Ca^{2+} ASW, we observed the same tendency for sperm, at the first UV flash only, to relocate their trajectories perpendicular to the flash axis. The absence of turning events and directed relocation of sperm paths along the flash axis correlated with the simultaneously measured inhibition of the fast rise in flagellar [Ca^{2+}]i. This implies that the turns, and the chemotaxis-like motility changes that they produce, are

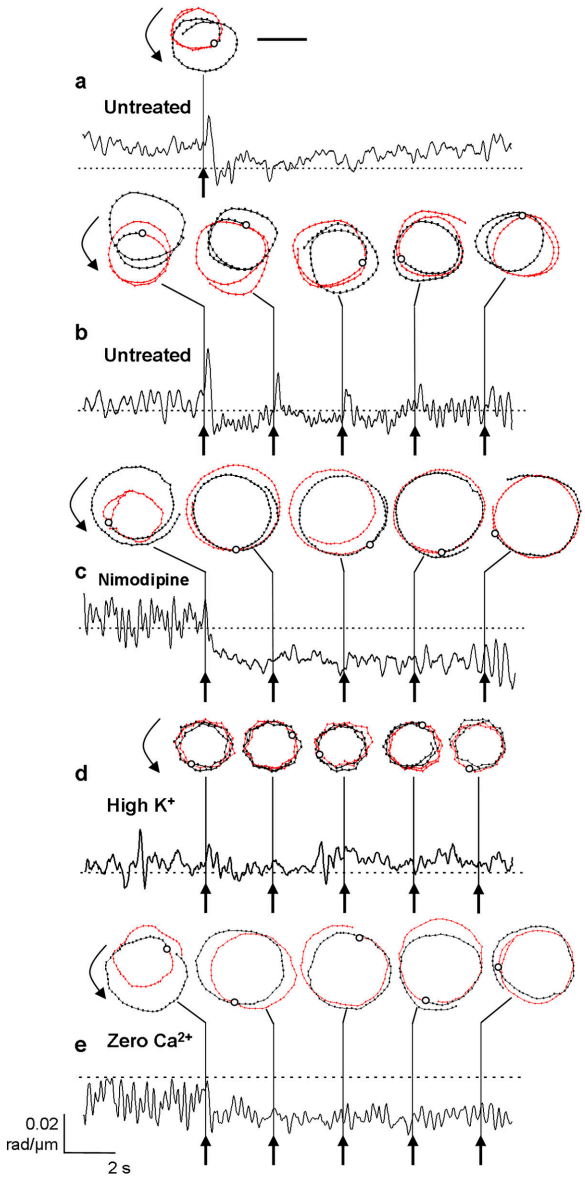

Figure 2. **Uncaging cGMP induces characteristic motility changes in single sperm.** (a) Trajectory of an individual caged cGMP-loaded sperm in ASW before (red) and after (black) a UV flash. Points along trajectory trace are 23 ms apart. Position of the sperm at the moment of UV flash is marked by a white circle. Bar, 60 μm. Curved arrow shows sperm swimming direction. Graph below shows curvature of sperm trajectory over time. Arrow and solid line indicate UV flash. Dashed line = 0.05 radians/μm. (b–e) Sperm trajectories during a series of UV flashes (b) ASW, (c) ASW containing 30 μM nimodipine, (d) high K^+ ASW, (e) zero Ca^{2+} ASW.

initiated by Ca^{2+} entry through opening of a nimodipine-sensitive pathway localized, or preferentially activated, in the flagella. The chemotaxis-like motility changes were also inhibited in the presence of 100–200 μM Ni^{2+} (Table I).

If the data in Fig. 4 b are a model of chemotaxis, a question to consider is why do sperm re-center their trajectories toward their position at the UV flash, and not in any other direction? Our interpretation is that a sperm swimming in a circle will first encounter a chemoattractant at the same point at which it is closest to the source. SAPs are known to elevate cGMP within ~50 ms (Kaupp et al., 2003), and we propose that, in our model system, the UV-stimulated increase in cGMP mimics the presence (and therefore direction) of a source of chemoattractant. This mechanism is repeated at successive UV flashes, which induce qualitatively similar directed relocations of the sperm. Their reduced size is possibly due to exhaustion of caged cGMP or desensitization of the signaling components to cGMP.

The best known and most widely studied targets for inhibition by DHPs such as nimodipine are Ca_v channels. Various members of this diverse family of Ca^{2+} channels have been identified in mammalian sperm and germ cells (for review see Darszon et al., 2005), and it is likely such diversity extends to sea urchin sperm. The nimodipine concentration used in this study (30 μM) is in a range reported to inhibit some T-type Ca_v channels (Akaike et al., 1989), and is several orders of magnitude greater than that commonly required to block L-type Ca_v channels. However, splice-variants of L-type channels with altered DHP-binding sites have been reported in rat sperm, and thus cannot be discounted as potential targets (Goodwin et al., 1998). Other putative targets potentially sensitive to nimodipine at the concentration used include K^+ channels and/or Cl^- channels (Chung and Kim, 2002; George Chandy et al., 2004). The concentration of nimodipine required to inhibit the chemotactic turns is also 3–6 times greater than that required to block the acrosome reaction in sea urchin sperm (Kazazoglou et al., 1985). DHPs have been shown to have multiple affinities for binding to sperm-derived membrane vesicles (Kazazoglou et al., 1985), indicating the presence of multiple binding sites and/or targets for DHPs in the sea urchin sperm. This could possibly explain the differing sensitivities of the two processes of motility and the acrosome reaction to inhibition by nimodipine.

Chemotactic turns are generated by transient increases in flagellar asymmetry. Current models assume that the degree of flagellar bend asymmetry varies in direct proportion to the flagellar $[Ca^{2+}]i$ (Cook et al., 1994; Kaupp et al., 2003; Ishikawa et al., 2004), as demonstrated in demembranated flagella (Brokaw, 1979). We used a novel fast fluorescence imaging system to observe that the flagella switch to a highly asymmetric state within 1 frame (or 23 ms, the maximum temporal resolution) of initiating an increase in $[Ca^{2+}]i$ (Fig. 3 a). The flagella then revert back to a less asymmetric conformation while the $[Ca^{2+}]i$ is still increasing (Fig. 3 a). It is unlikely that this is due to a lag in the dye reporting $[Ca^{2+}]i$ decreases, as the closely related dye fluo-3 has a reported time constant of decay of ~5–10 ms (Escobar et al., 1997). We therefore propose a new model for the regulation of flagellar symmetry, whereby the flagella are not sensitive to the overall $[Ca^{2+}]i$, per se, but increase their asymmetry due to the entry of extracellular Ca^{2+} through a nimodipine-sensitive pathway located in the flagella. Ca^{2+} entry itself is required to increase flagellar asymmetry and generate turns (Fig. 2 e), ruling out the possibility that the sensor transmitting information to the flagellum is activated solely by a conformational change of a Ca^{2+}-conducting channel or exchanger. Intriguingly, this sensor is somehow able to discriminate between $[Ca^{2+}]i$ entering via a nimodipine-sensitive pathway, and $[Ca^{2+}]i$ increases resulting from activation of separate Ca^{2+} entry pathway(s) during the "plateau" phase (Fig. 1, e and f; Fig. 2 c). One possibility is that the sensor for

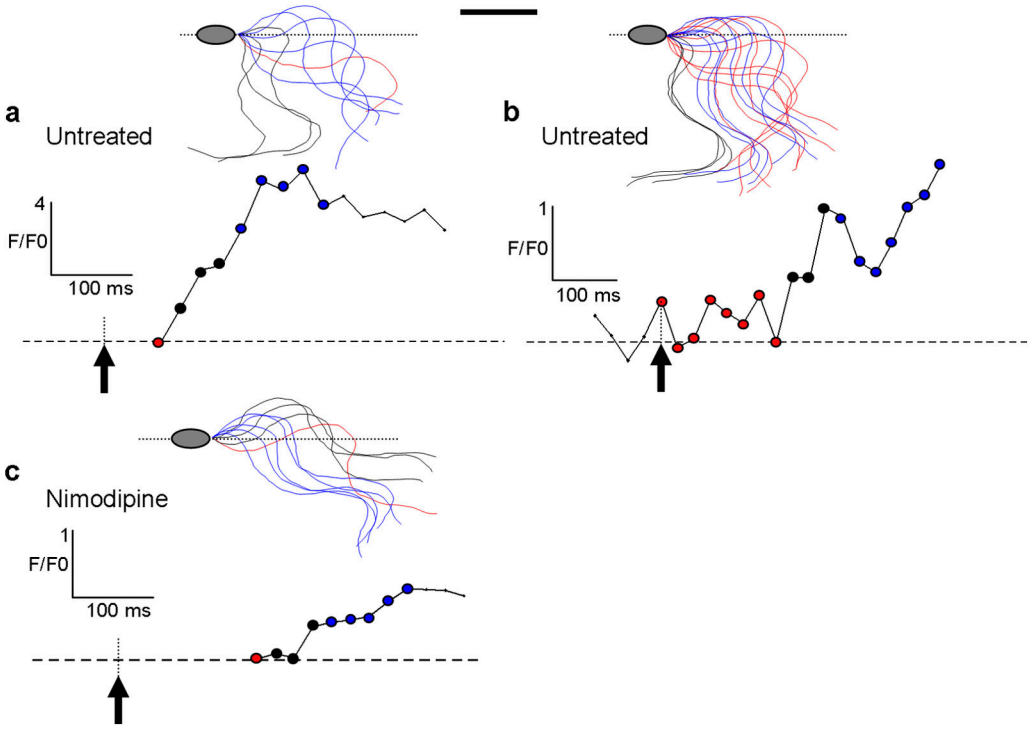

Figure 3. **Momentary increases in flagellar asymmetry accompany the fast, transient increase in flagellar [Ca^{2+}]i and are inhibited by nimodipine.** (a) Top panel shows position of the flagellum from an untreated single sperm in relation to a normalized head axis. Red trace is from first visible image of the flagellum after initial, or first, UV flash. Black traces are the position of the same flagellum in the subsequent three images. Blue traces are the position of the flagellum in final five images presented. Position of flagellum recorded every 23 ms. Bar, 10 μm. Dashed line indicates long axis of head. Bottom panel shows [Ca^{2+}]i increase in flagellum shown above. Points are color-coded to corresponding traces. Arrow with line denotes UV flash. Dashed line indicates F/F_0 value of 1. (b) Position of flagella from untreated cGMP-loaded sperm after a secondary UV flash. Color coding of flagellum, scale, and interval between flagellum traces as in panel a. Bottom panel shows [Ca^{2+}]i increase in flagellum shown above. Color coding, UV flash as in panel a. Dashed line shows an F/F_0 value of 3. (c) Sperm in ASW containing 30 μM nimodipine. Color coding of flagellum, scale, and interval between flagellum traces as in panel a. Bottom panel shows [Ca^{2+}]i increase in flagellum shown above. Color coding, UV flash, and dashed line as in panel a.

the flagellum might detect localized Ca^{2+} increases within the immediate vicinity of, for example, nimodipine-sensitive Ca_v channels, suggesting a close spatial association of the two components. Alternatively, the flagellum may be sensitive to the rate of change of [Ca^{2+}]i, increasing its asymmetry only in response to the rapid increase in [Ca^{2+}]i produced by activation of the nimodipine-sensitive pathway. Furthermore, the subsequent prolonged switch to a less asymmetrical flagellar conformation is not the result of a decrease in [Ca^{2+}]i as current models have suggested (Kaupp et al., 2003; Ishikawa et al., 2004), as it occurs against a background of elevated [Ca^{2+}]i (Fig. 1, c–f; Fig. 2). Neither is it stimulated by Ca^{2+} entry, as it occurs in the absence of extracellular Ca^{2+} (Fig. 2 e). This switch to straighter-swimming paths could therefore be mediated by cGMP-stimulated alteration of another cellular parameter, such as intracellular pH, cAMP levels, or membrane potential.

In summary, we have simultaneously measured [Ca^{2+}]i and flagellar form in swimming sea urchin sperm, and found that activation of a nimodipine-sensitive pathway is required to increase flagellar asymmetry and produce chemotaxis-like motility changes. These data challenge long-standing assumptions regarding the relationship between overall [Ca^{2+}]i and flagellar asymmetry and have significant implications for the regulation of flagellar movement in other biological systems.

Materials and methods

Materials

Sperm were obtained "dry" from *S. purpuratus* (Marinus Inc.) by intercoelomic injection of 0.5 M KCl, and were stored on ice. ASW, zero Ca^{2+} ASW, and high K^+ ASW were prepared as described (Wood et al., 2003). Fluo-4-AM, FM1-43, and Pluronic F-127 were from Molecular Probes, Inc. Esterified caged cyclic GMP (Bhc-cGMP/Ac) was synthesized using 6-bromo-7-hydroxycoumarin-4-ylmethyl as the caging group (Furuta et al., 2004). Nimodipine was from Tocris Cookson Inc. PolyHEMA (poly(2-hydroxyethyl methacrylate)) was from Sigma-Aldrich.

Loading of fluorescent indicators and caged compounds

Sperm were prepared as previously described (Wood et al., 2003), with the exception that after the first hour of incubation at 15°C, Bhc-cGMP/Ac was added to a final concentration of 50 μM, and samples incubated for a further 1 h at 15°C. For Fig. S2, sperm were loaded for 1 h at 15°C with Bhc-cGMP/Ac, with 10 μM FM1-43 added for the final 15 min.

Fluorescence imaging of swimming sperm

All coverslips were briefly immersed into a 0.05–0.1% (wt/vol) solution of polyHEMA in ethanol, hot-air blow-dried to rapidly evaporate the solvent, and mounted in supplied reusable chambers to fit a TC-202 Bipolar temperature controller (Medical Systems Corp.). The temperature plate was mounted on a microscope stage (Eclipse TE 300; Nikon) and maintained at a constant 15°C. 1-μl aliquots of labeled sperm were diluted in 2.5 × 10^5 volumes of the appropriate ASW, and were transferred to an imaging chamber. Epifluoresence images were collected with a Nikon Plan Apo 60× 1.4 NA objective using a Chroma filter set (ex, HQ470/40×; DC, 505DCXRU; em, HQ510LP) and were recorded on a CCD camera (Quantix 57; Photometrics Inc.). Fluorescence illumination was supplied by a Luxeon V Star Lambertian Cyan LED part # LXHL-LE5C (Lumileds Light-

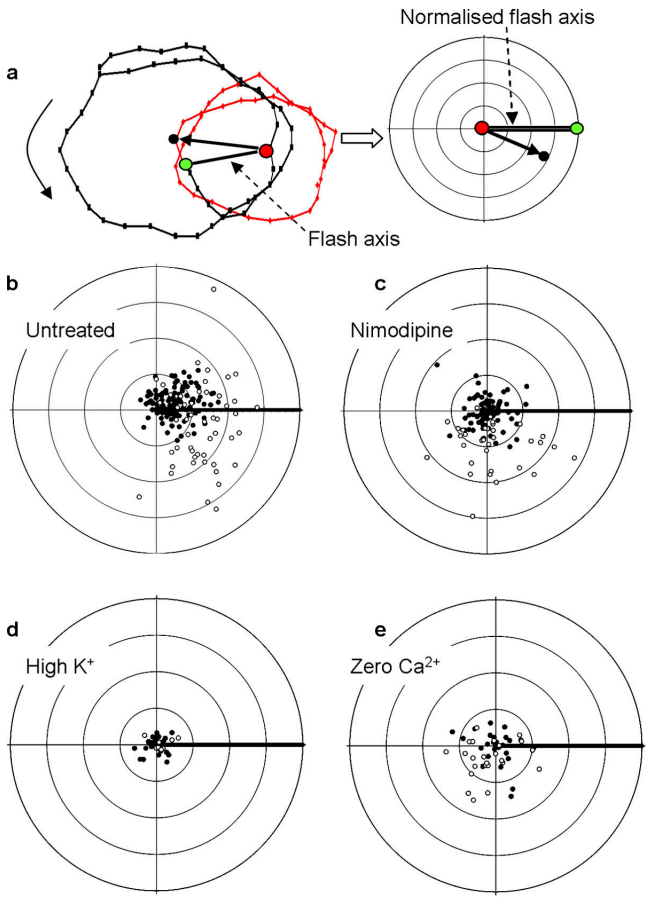

Figure 4. **Uncaging of cGMP induces a directed relocation of sperm toward a hypothetical stimulus source.** (a) Schematic depiction of the calculation of the distance and angle data in the polar plots. The flash axis (black line) is defined by the center of the sperm circular trajectory before the UV flash (red circle) and the position of the sperm at which it receives a UV flash (green circle). The center of the sperm circular trajectory after the UV flash (black circle) is then described by two variables: its displacement from the center of circling before uncaging of cGMP (the length of the arrow) and its angular displacement from the flash axis. The origins of the polar graphs are the center of the sperm circular trajectory before the UV flash, with the flash axis normalized as the 0° axis for each individual UV flash. Curved arrow shows sperm swimming direction. (b) Relocation of sperm after uncaging of cGMP in sperm in ASW. Concentric circles at 10-μm intervals. Open circles = relocation of the center of the circular swimming path after first UV flash; closed circles = relocation of the center of the circular swimming path up to a maximum of four subsequent UV flashes per sperm (i.e., applied after first UV flash). (c) Sperm in ASW containing 30 μM nimodipine. (d) Sperm in high K^+ ASW. (e) Sperm in zero Ca^{2+} ASW.

ing LLC) attached to a custom-built stroboscopic control box. The LED was mounted into a FlashCube40 assembly with dichroic mirror M40-DC400 (Rapp Opto Electronic). Photolysis of the caged compounds was achieved using a UV flash lamp system, (JML-C2; Rapp Opto Electronic) with a UV band-pass filter (270–400 nm) connected to the FlashCube40 side-port via a liquid light guide (2 mm, 0.45 NA). Output energy of the flash lamp was fixed in all experiments (total energy per flash, 135 J). LED output was synchronized to the Exposure Out signal of the Quantix 57 camera via the control box to produce a single flash of 1 ms duration per individual exposure (see Fig. S3 for a schematic diagram of the imaging equipment). The camera exposure time was set equivalent to flash duration (1 ms). In full-chip mode with 4 × 4 binning the camera read-out time is 22 ms, therefore images were collected every 23 ms with exposure time to fluorescence illumination of 1 ms per image. Images were collected with AQM Advance 6 software (Andor Bioimaging). UV flashes were triggered by a BoB unit (Andor Bioimaging) connected to a Master 8 pulse generator (A.M.P.I.).

Image processing

Sperm head trajectories, sperm velocities, and sperm head fluorescence were measured using Objects module of Motion Analysis and Tracking software (Andor Bioimaging). Sperm trajectory curvature was measured using BohBoh software (BohBohSoft) using an n-span (smoothing value) of 2 for calculations presented in Table I, and 4 for graphs in Fig. 2 (Baba and Mogami, 1985). Flagella curvature and fluorescence were measured using the Autotrace module of BohBoh software. In Figs. 1 and 3 the change in $[Ca^{2+}]i$ in the flagellum is stated as F/F_0, where the F_0 value is taken from the first image in which the flagellum is visible after the UV flash. Due to the inability to measure basal $[Ca^{2+}]i$ in flagella, these values are an underestimation of the true relative increase of $[Ca^{2+}]i$ occurring in the flagella.

Statistical analyses

Data are presented from sperm collected from a minimum of three urchins. Statistical significance was derived from REGWQ iterative multiple comparisons test (95% confidence interval) and confirmed with Dunnett's test (two-tailed, 95% confidence interval) with either untreated condition or high K^+ condition used as control as appropriate.

Online supplemental material

Fig. S1 depicts swimming velocity of sperm before and after UV uncaging of cGMP in untreated and nimodipine-treated sperm, and in sperm swimming in zero Ca^{2+} or high K^+ ASW. Fig. S2 shows the changes in flagellar asymmetry provoked by uncaging of cGMP in a sperm loaded with the membrane dye FM1-43. Fig. S3 is a schematic diagram of the imaging system. Video 1 is a synchronized montage of fluorescence images of an untreated sperm and a nimodipine-treated sperm, swimming before and after UV-mediated release of cGMP. Images from Video 1 are shown individually in Fig. 1. Video 2 shows an untreated sperm receiving multiple UV flashes over ~17 s. Video 3 shows a nimodipine-treated sperm receiving multiple UV flashes over ~17 s. Online supplemental material available at http://www.jcb.org/cgi/content/full/jcb.200411001/DC1.

We would like to thank Arturo Hernández-Cruz, Claudia Martínez-Anaya, Victor Vacquier, Michael Whitaker, and Michael White for helpful comments and suggestions during the preparation of this manuscript.

The work was supported in part by grants from The Wellcome Trust, CONACyT, DGAPA (UNAM), and UC MEXUS. The authors declare that they have no competing financial interests.

Submitted: 1 November 2004
Accepted: 29 April 2005

References

Akaike, N., P.G. Kostyuk, and Y.V. Osipchuk. 1989. Dihydropyridine-sensitive low-threshold calcium channels in isolated rat hypothalamic neurones. *J. Physiol.* 412:181–195.

Baba, S.A., and Y. Mogami. 1985. An approach to digital image analysis of bending shapes of eukaryotic flagella and cilia. *Cell Motil. Cytoskeleton.* 5:475–489.

Brokaw, C.J. 1974. Calcium and flagellar response during the chemotaxis of bracken spermatozoids. *J. Cell. Physiol.* 83:151–158.

Brokaw, C.J. 1979. Calcium-induced asymmetrical beating of triton-demembranated sea urchin sperm flagella. *J. Cell Biol.* 82:401–411.

Chung, M.K., and H. Kim. 2002. Volume-activated chloride currents from human fibroblasts: blockade by nimodipine. *Gen. Physiol. Biophys.* 21:85–101.

Cook, S.P., and D.F. Babcock. 1993. Activation of Ca^{2+} permeability by cAMP is coordinated through the pHi increase induced by speract. *J. Biol. Chem.* 268:22408–22413.

Cook, S.P., C.J. Brokaw, C.H. Muller, and D.F. Babcock. 1994. Sperm chemotaxis: egg peptides control cytosolic calcium to regulate flagellar responses. *Dev. Biol.* 165:10–19.

Cosson, J., P. Huitorel, and C. Gagnon. 2003. How spermatozoa come to be confined to surfaces. *Cell Motil. Cytoskeleton.* 54:56–63.

Cosson, M.P., D. Carre, and J. Cosson. 1984. Sperm chemotaxis in siphonophores. II. Calcium-dependent asymmetrical movement of spermatozoa induced by the attractant. *J. Cell Sci.* 68:163–181.

Darszon, A., T. Nishigaki, C. Wood, C.L. Trevino, R. Felix, and C. Beltran. 2005. Calcium channels and Ca^{2+} fluctuations in sperm physiology. *Int. Rev. Cytol.* 243:79–172.

Doering, C.J., and G.W. Zamponi. 2003. Molecular pharmacology of high voltage-activated calcium channels. *J. Bioenerg. Biomembr.* 35:491–505.

Eisenbach, M. 1999. Sperm chemotaxis. *Rev. Reprod.* 4:56–66.

Escobar, A.L., P. Velez, A.M. Kim, F. Cifuentes, M. Fill, and J.L. Vergara. 1997. Kinetic properties of DM-nitrophen and calcium indicators: rapid transient response to flash photolysis. *Pflugers Arch.* 434:615–631.

Furuta, T., H. Takeuchi, M. Isozaki, Y. Takahashi, M. Kanehara, M. Sugimoto, T. Watanabe, K. Noguchi, T.M. Dore, T. Kurahashi, et al. 2004. Bhc-cNMPs as either water-soluble or membrane-permeant photoreleasable cyclic nucleotides for both one- and two-photon excitation. *ChemBioChem.* 5:1119–1128.

George Chandy, K., H. Wulff, C. Beeton, M. Pennington, G.A. Gutman, and M.D. Cahalan. 2004. K^+ channels as targets for specific immunomodulation. *Trends Pharmacol. Sci.* 25:280–289.

Gonzalez-Martinez, M.T., B.E. Galindo, L. de De La Torre, O. Zapata, E. Rodriguez, H.M. Florman, and A. Darszon. 2001. A sustained increase in intracellular Ca^{2+} is required for the acrosome reaction in sea urchin sperm. *Dev. Biol.* 236:220–229.

Goodwin, L.O., N.B. Leeds, I. Hurley, G.W. Cooper, R.G. Pergolizzi, and S. Benoff. 1998. Alternative splicing of exons in the α1 subunit of the rat testis L-type voltage-dependent calcium channel generates germ line-specific dihydropyridine binding sites. *Mol. Hum. Reprod.* 4:215–226.

Harumi, T., K. Hoshino, and N. Suzuki. 1992. Effects of sperm-activating peptide I on *Hemicentrotus pulcherrimus* spermatozoa in high potassium sea water. *Dev. Growth Differ.* 34:163–172.

Ishikawa, M., H. Tsutsui, J. Cosson, Y. Oka, and M. Morisawa. 2004. Strategies for sperm chemotaxis in the siphonophores and ascidians: a numerical simulation study. *Biol. Bull.* 206:95–102.

Kaupp, U.B., J. Solzin, E. Hildebrand, J.E. Brown, A. Helbig, V. Hagen, M. Beyermann, F. Pampaloni, and I. Weyand. 2003. The signal flow and motor response controling chemotaxis of sea urchin sperm. *Nat. Cell Biol.* 5:109–117.

Kazazoglou, T., R.W. Schackmann, M. Fosset, and B.M. Shapiro. 1985. Calcium channel antagonists inhibit the acrosome reaction and bind to plasma membranes of sea urchin sperm. *Proc. Natl. Acad. Sci. USA.* 82:1460–1464.

Miller, R. 1985. Sperm chemo-orientation in the metazoa. *In* Biology of Fertilization. C. Metz and A. Monroy, editors. Academic Press Inc., New York. 275–337.

Miller, R.L., and C.J. Brokaw. 1970. Chemotactic turning behaviour of *Tubularia spermatozoa. J. Exp. Biol.* 52:699–706.

Nishigaki, T., C.D. Wood, Y. Tatsu, N. Yumoto, T. Furuta, D. Elias, K. Shiba, S.A. Baba, and A. Darszon. 2004. A sea urchin egg jelly peptide induces a cGMP-mediated decrease in sperm intracellular Ca^{2+} before its increase. *Dev. Biol.* 272:376–388.

Shimomura, H., and D.L. Garbers. 1986. Differential effects of resact analogues on sperm respiration rates and cyclic nucleotide concentrations. *Biochemistry.* 25:3405–3410.

Spehr, M., G. Gisselmann, A. Poplawski, J.A. Riffell, C.H. Wetzel, R.K. Zimmer, and H. Hatt. 2003. Identification of a testicular odorant receptor mediating human sperm chemotaxis. *Science.* 299:2054–2058.

Suzuki, N., and D.L. Garbers. 1984. Stimulation of sperm respiration rates by speract and resact at alkaline extracellular pH. *Biol. Reprod.* 30:1167–1174.

Ward, G.E., C.J. Brokaw, D.L. Garbers, and V.D. Vacquier. 1985. Chemotaxis of *Arbacia punctulata* spermatozoa to resact, a peptide from the egg jelly layer. *J. Cell Biol.* 101:2324–2329.

Wood, C.D., A. Darszon, and M. Whitaker. 2003. Speract induces calcium oscillations in the sperm tail. *J. Cell Biol.* 161:89–101.

Yunker, A.M. 2003. Modulation and pharmacology of low voltage-activated ("T-Type") calcium channels. *J. Bioenerg. Biomembr.* 35:577–598.